POTENTIAL FIELD CELLULAR AUTOMATA MODEL FOR OVERCROWDED PEDESTRIAN FLOW

Peng Zhang[1, 5*], Xiao-Yang Li[1, 5], Hua-Yu Deng[1], Zhi-Yang Lin[2], Xiao-Ning Zhang[3], S.C. Wong[4]
[1] *Shanghai Institute of Applied Mathematics and Mechanics, Shanghai University, Shanghai, China*
[2] *Department of Aeronautics and Astronautics, Fudan University, Shanghai, China*
[3] *School of Economics and Management, Tongji University, Shanghai, China*
[4] *Department of Civil Engineering, The University of Hong Kong, Hong Kong SAR, China*
[5] *Shanghai Key Laboratory of Mechanics in Energy Engineering, Shanghai, China*

Abstract: We propose a cellular automata model for overcrowded pedestrian flow in which we divide a normal cell of size 0.4 m × 0.4 m into nine small cells. The compressibility between pedestrians is such that a refined central cell refers to only one pedestrian, and a refined side or corner cell of this pedestrian can be shared respectively by at most one or three other pedestrians. The compressibility between a pedestrian and a wall is also taken into account, which is reasonably half as much as that between pedestrians. Therefore, the model allows a density exceeding 10 ped/m^2, which has been observed in crowd disasters. A pedestrian's movement is assumed to minimize the deviation from the negative gradient of cost potential, along which the travel cost for moving a unit distance is minimized. Moreover, the probability of movement is assumed to decrease along with the minimal travel cost and derivation, which significantly improves the rules presented in two previous works. As a result, the simulated fundamental diagram and evacuation process generally agree with field studies in the literature. For two pedestrian groups, the cost is increased for their confrontation and mingling with each other, which helps reproduce the segregation and formation of lanes in counter-flow. However, the degree depends on the magnitude of increased cost and the density, which is measured by the probability of gridlock and order parameter through simulation.

Keywords: cost distribution; refined cells; evacuation; counter-flow; lane formation.

1. INTRODUCTION

Pedestrian dynamics have attracted researchers in many disciplines. From a macroscopic view, pedestrian flow is considered a continuum, and hydrodynamic equations are used for modeling (Hughes 2002; Hoogendoorn and Bovy 2004; Huang et al. 2009; Xia, Wong, and Shu 2009; Jiang et al. 2010; Xiong et al. 2011). From a microscopic view, pedestrians are particles in motion. In a many-particle or social-force model (Helbing and Molnár 1995; Helbing et al. 2001; Helbing 2001), accelerations of all "particles" are established to constitute an ordinary differential system, which takes into account the self-driven force of each particle to the destination and the repulsive forces among all particles. The social-force model is widely applied to many practical problems, e.g., in Porter, Hamdar, and Daamen (2018) and Zhou et al. (2019). In a cellular automaton (CA) model (Burstedde et al. 2001; Kirchner and Schadschneider 2002; Kirchner, Nishinari, and Schadschneider 2003; Nishinari et al. 2004; Varas et al. 2007; Kirik, Yurgel'yan, and Krouglov 2009; Huang and Guo 2008; Kretz 2009; Kretz 2010; Hartmann 2010; Zhang et al. 2012), also called a lattice-gas automaton model (see Kuang et al. 2008; Kuang et al. 2014; Li and Dong 2012, and the references therein), the walking domain is divided into grid cells and a "particle" updates its position at each time step. In general, pedestrian flow is analogous to vehicular flow in terms of follow-the-leader and self-organized behavior. However, the problem is two-dimensional and pedestrians' path-choice strategy is essential for modeling.

The floor field (Burstedde et al. 2001; Kirchner and Schadschneider 2002; Huang and Guo 2008) and potential field (Varas et al. 2007; Kretz 2010; Hartmann 2010; Zhang et al. 2012) are useful for modeling pedestrians' navigation to a destination in a CA model. The floor field includes a static and a dynamic field. The former measures the Euclidean distance between a given cell and the destination, and the latter measures the trace left by pedestrians in the cell, together with its decay and diffusion. The values of static and dynamic fields are incorporated in a formula to reflect the attractiveness of the cell. The more attractive a cell is, the higher the probability that pedestrians in neighboring cells will

occupy it. The potential field suggests the lowest cost for a pedestrian to travel from his/her current position to the destination. Because it is assumed that pedestrians are familiar with the walking domain and thus are able to minimize their costs, a pedestrian takes the direction of motion as the negative gradient of potential in his/her current position. This principle has been used in macroscopic models (Hughes 2002; Huang et al. 2009; Xia, Wong, and Shu 2009; Jiang et al. 2010), and in a recently proposed CA model (Zhang et al. 2012). Similar principles for finding a quickest path have also been proposed for CA models (Kirchner, Nishinari, and Schadschneider 2003; Kretz 2009; Guo, Huang, and Wong 2013). However, all of these formulations are analogous to those for optical propagation, which directly result in or are indirectly associated with the eikonal equation.

The CA models noted above can simulate many typical phenomena of pedestrian flow, such as movement through a corridor, evacuation from a room, and formation of lanes in counter-flow. However, these models (together with many other similar models) assume that each cell is occupied by at most one pedestrian, who is thus able to update his/her position simply by moving to an empty neighboring cell. In this case, the size of a cell is normally supposed to be 0.4 m × 0.4 m, which suggests a maximal density of 6.25 ped/m^2, according to the stated occupation rule. These formulations do not reflect interaction due to physical contact between pedestrians, and the value of the maximal density is too small to reflect overcrowded situations. Observations show that the density may reach over 10 ped/m^2, especially before or when a crowd disaster takes place, in which case the motion of the crowd does not entirely cease (Helbing, Johansson, and Al-Abideen 2007; Helbing and Mukerji 2012). Therefore, these CA models should be improved or extended to describe overcrowded pedestrian flow. Kirchner et al. (2004) improved the floor field CA model by reducing the cell size from 0.4 m × 0.4 m to 0.2 m × 0.2 m, and allowing a pedestrian to occupy more than one cell. However, the maximal density was still set as 6.25 ped/m^2. Based on a study by Zhang et al. (2012), Jian et al. (2014) extended the potential field CA model to a walking domain with poor visibility, by introducing an aggregate force field and allowing a 0.4 m × 0.4 m cell to be occupied by at most two pedestrians. Xie et al. (2012) similarly allowed a 0.5 m × 0.5 m cell to be shared by two pedestrians. Although the maximal density was doubled to accommodate overcrowding situations, the unrefined cell and update time made little improvement in spatial and temporal continuity.

The present paper proposes a multi-grid potential field CA model, which significantly improves on the models in Zhang et al. (2012) and Jian et al. (2014). By dividing a normal cell of size 0.4 m × 0.4 m into nine smaller cells of size (0.4 m × 0.4 m)/9 and the time step 0.4 s into three intervals without change in movement speed ($v_m \approx 1$ m/s), we can greatly enhance the continuity of modeling. It is worth noting that similar discrete cells were used to simulate emergency or panic evacuations in Song et al. (2006), Weng et al. (2007), Zhang, Song, and Xu (2008), Chen, Han, and Zhang (2011), Fang et al. (2012), and Ibrahim, Venkat, and Wilde (2018). Among the refined nine cells that are occupied by one pedestrian, the central cell cannot be shared by another pedestrian, whereas each of the four side cells can be shared by at most one other pedestrian and each of the four corner cells can be shared by at most three other pedestrians. This restriction is equivalent to assuming that the distance between the central points of any two pedestrians cannot be shorter than 0.4 m/3, which suggests reasonable compressibility for physical contacts between pedestrians. The compressibility between a pedestrian and a wall (or an obstacle) is also taken into account, which is reasonably half as much as that between pedestrians. Therefore, the improved model is able to simulate overcrowded pedestrian flow, in that the maximal density reaches $\rho_{max} = 14$ ped/m^2.

Although a pedestrian's direction of motion is determined similarly to that in Zhang et al. (2012), the probability of movement is assumed to decreasingly depend on the minimized travel cost along the negative gradient of cost potential and the minimized deviation from the negative gradient. This actually suggests a reasonable speed–density relationship, and significantly improves the update rules in Zhang et al. (2012) and Jian et al. (2014). As a consequence, the simulated fundamental diagrams and maximal flow rates through an exit agree well with the observed data. In contrast, we find no parameters for the models in Zhang et al. (2012) and Jian et al. (2014) to fit the observed data, according to the simulation. The procedure of the proposed model can be briefly described as follows:

(1) Reconstruct the density of each cell by taking the weighted average of pedestrians in the surroundings;

(2) Derive the potentials of all cells by solving the eikonal equation, in which the cost distribution measures the traveling time and discomfort for moving a unit distance;

(3) Determine the candidate cells for a pedestrian's movement, obeying the stated occupation rule;
(4) Select the target cells from the candidate cells, to which the movement would bring about a reduction in potential greater than moving to any other candidate cell; and
(5) Determine the pedestrian's movement: he/she moves to one of the target cells with a probability that is generally smaller than that in Zhang et al. (2012) and decreasingly depends on the pedestrian's discomfort and the deviation of moving direction from the negative gradient of the potential.

Because serial updating is adopted, there are no conflicts for two or more pedestrians moving to the same cell. The scenario in which two pedestrian groups with different destinations mingle is also formulated by assuming larger costs for their mingling, which together with the enhanced continuity allows the formation of lanes in counter-flow to be reproduced, even for a high average density of over 5 ped/m^2. Compared with the formulation used in Jian et al. (2014), our formulation is more robust, adopting simple dynamics and allowing for efficient implementation.

Although the refinement of cells and the assumption on compressibility are generally suitable, we note that the optimal path-choice strategy formulated in the present paper is mainly for overcrowd pedestrian flow under normal conditions, which is not directly applicable to crowds in other situations, e.g., panicking, in the dark, or with reduced visibility.

The remainder of this paper is organized as follows. In Section 2, the division of a walking domain is discussed, as are the basic rules for occupation and a pedestrian's updating of his/her position. In Section 3, the path-choice strategy based on the potential field is discussed in detail. Numerical results are given in Section 4, and the paper is concluded in Section 5.

2. FUNDAMENTALS

The walking domain is divided into small cells of size (0.4 m × 0.4 m)/9. We assume that one pedestrian optimally occupies nine refined cells if none of these cells are occupied by other pedestrians. This case indicates a non-overcrowded situation without physical contacts, or a density of less than 6.25 ped/m^2. In an overcrowded situation, or when the density is greater than 6.25 ped/m^2, some cells must be shared by more than one pedestrian.

2.1 Basic Rules for Occupation of Cells and Walking Domain

Among the nine refined cells occupied by a pedestrian, the cell at the center is called the central cell and the others are controlled cells. The eight controlled cells include four side and four corner cells (Figure 1). If these cells are not occupied by other pedestrians, then each cell contains 1/9 pedestrians (Figure 1(a)). A controlled cell can be occupied by more than one pedestrian, whereas a central cell can never be shared by another pedestrian. This occupation rule is fundamental, as it implies that the central cells of any two pedestrians must remain at least two cells apart.

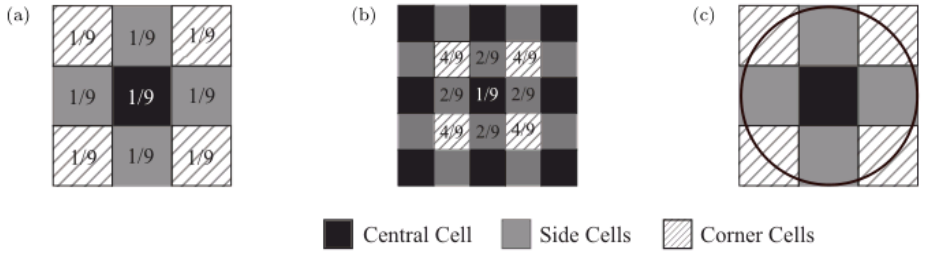

Figure 1. Cells occupied by pedestrians. (a) Nine refined cells occupied by just one pedestrian, in which case each cell contains 1/9 pedestrians; (b) The most overcrowded situation: a central, side, or corner cell can be occupied by at most one, two, or four pedestrians, respectively; (c) The area occupied by a pedestrian in a side cell is almost twice that of a corner cell, which implies that the maximal occupancy of a corner cell is almost twice as much as that of a side cell.

Regarding a pedestrian and his/her central cell, the most overcrowded situation is shown in Figure 1(b). We observe that side and corner cells can be occupied by at most two and four pedestrians, respectively. In this case, they contain 2/9 and 4/9 pedestrians, respectively. Figure 1(c) shows that the

maximal occupancy of a corner cell is twice that of a side cell. We observe that the area of a side cell occupied by one pedestrian is almost twice that of a corner cell. Therefore, we assume that the compressibility of a corner cell is twice that of a side cell. Here, the projection of a pedestrian onto the ground is taken as an approximate circle with diameter of 0.4 m.

We also take into account the compressibility between pedestrians and walls (or other obstacles), by assuming that the first layer of artificial cells is half within the wall and half within the walking domain. Half of an artificial cell within the domain is either empty or controlled by at most one pedestrian (or two pedestrians) as half of a side (or corner) cell (Figure 2). These assumptions imply that the compressibility between pedestrians and walls is half that between pedestrians because walls are completely incompressible. In this regard, these are also called semi-artificial cells. Assume a rectangular walking domain containing $(2M-1) \times (2N-1)$ inner cells, which has the area $2M \cdot 2N \cdot 0.16/9$ m^2. We observe that the domain can contain at most MN pedestrians, in which case the globally maximal density reaches $9MN/(0.16 \cdot 2M \cdot 2N)$ ped/$m^2 \approx 14.06$ ped/m^2.

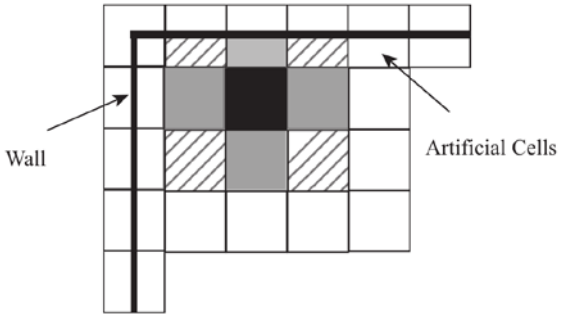

Figure 2. Division of the walking domain. The first layer of artificial cells is half within the wall and half within the domain. The half within the domain can be occupied by pedestrians' controlled cells.

2.2 Basic Rules for Updating a Pedestrian's Position

For the motion of a pedestrian, we only consider the central part, and assume that the eight controlled parts move in parallel. Referring to Figure 1(a), we assume that a central part either keeps still or moves to one of the controlled neighboring cells at each time step.

In time step n, the serial update is implemented with all $K(n)$ pedestrians in the walking domain being randomly numbered $k = 1, \ldots, K(n)$. For the k-th pedestrian, we denote the central cell by (0,0), and the eight neighboring controlled cells by (i,j), $i,j = 0,\pm 1$, $i^2 + j^2 \neq 0$. Here, (0,0) and (i,j) also denote the coordinates of central points of these cells, which are scaled by cell length. Under the basic rule for occupation (Section 2.1), the central part of the k-th pedestrian may only move to (i,j) if none of the cells newly occupied by him/her are the central cells of any others after movements for the previous $k-1$ pedestrians have been ascertained. In this case, (i,j) is called a candidate cell of the k-th pedestrian.

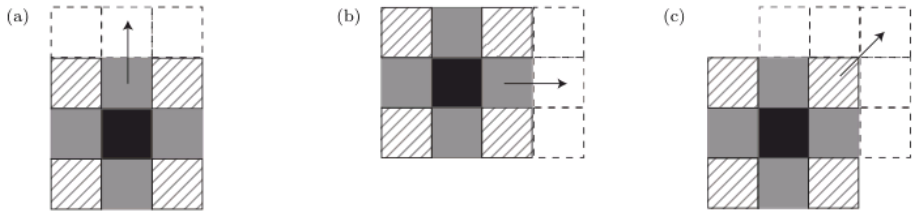

Figure 3. Updating a pedestrian's position. The central part (a) moves to a side cell along the y axis; (b) moves to a side cell along the x axis; (c) moves to a corner cell.

To find all candidate cells of the k-th pedestrian, three cases are considered for movement to the eight neighboring controlled cells (i,j): (i) $i = 0$, $j \neq 0$, i.e., the movement is parallel to the y axis (Figure 3(a)); (ii) $i \neq 0$, $j = 0$, i.e., the movement is parallel to the x axis (Figure 3(b)); and (iii) $ij \neq 0$, i.e., (i,j) is a corner cell (Figure 3(c)). For these movements, the cells newly occupied by the pedestrian are indicated as follows: (i) $S_y = \{(i,2j),(i-1,2j),(i+1,2j)\}$; (ii) $S_x = \{(2i,j),(2i,j-1),(2i,j+1)\}$; and (iii) $S_{xy} = \{(2i,0),(2i,j),(2i,2j),(i,2j),(0,2j)\}$.

Let the value $\upsilon(x,y)$ be assigned to a cell (x,y), such that $\upsilon(x,y) = 0$ if (x,y) is empty, $\upsilon(x,y) = 1$ if (x,y) is a central cell, and $\upsilon(x,y) = 0.5$ if (x,y) is a controlled cell. Then, we can easily verify that (i,j) is

a candidate cell if and only if

(1) $i = 0, j \neq 0$, and $\prod_{(\xi,\eta)\in Sy}(\upsilon(\xi,\eta) - 1) \neq 0$; or

(2) $i \neq 0, j = 0$, and $\prod_{(\xi,\eta)\in Sx}(\upsilon(\xi,\eta) - 1) \neq 0$; or

(3) $ij \neq 0$, and $\prod_{(\xi,\eta)\in Sxy}(\upsilon(\xi,\eta) - 1) \neq 0$.

The set of candidate cells is denoted by S_c, which may be empty or contain more than one element. In the former case, the pedestrian does not move. In the latter case, the pedestrian either keeps still or uniquely selects a cell from S_c to move to, depending on the cost potential field at that moment.

3. COST POTENTIAL FIELD AND PATH-CHOICE STRATEGY

For a pedestrian in position (x,y) and at time t, walking a small distance ds gives rise to the cost $c(x,y,t)ds$, which is associated with travel time and mingling with other pedestrians through the definition of the cost distribution:

$$c(x, y, t) = 1/v_m + g(\rho(x, y, t)). \tag{1}$$

Here, $v_m = 1$ m/s is the walking speed, and thus the cost ds/v_m measures the traveling time; $g(\rho)$ is the discomfort for traveling a unit distance, and thus the cost $g(\rho)ds$ measures the discomfort in the journey. The discomfort is ascribed to crowdedness; thus we have $g(0) = 0$, and $g'(\rho) > 0$.

3.1 Eikonal Equation and Cost Potential

Assume that all pedestrians in the walking domain uniformly have destination Γ_0. Then, if t is fixed, there uniquely exists a function $\phi(x,y) > 0$, which solves the following eikonal equation:

$$\sqrt{\phi_x^2(x, y) + \phi_y^2(x, y)} = c(\rho(x, y)), \quad \phi(x_0, y_0) = 0, \quad \text{for } (x_0, y_0) \in \Gamma_0. \tag{2}$$

Here and hereafter, we omit the argument t for simplicity in discussion. It is well known that $\phi(x,y)$ reduces with the maximal rate along the direction of the negative gradient $-(\phi_x,\phi_y) \equiv -\nabla\phi$, as is indicated by the derivative of $-\phi(x,y)$ in the direction $(v_1(x,y), v_2(x,y))$,

$$\lim_{\Delta s\to 0} \frac{\phi(x, y) - \phi(x + \Delta x, y + \Delta y)}{\Delta s} = -\phi_x v_1 - \phi_y v_2 \le \sqrt{(-\phi_x)^2 + (-\phi_y)^2} = c, \tag{3}$$

where the increments $\Delta x = v_1\Delta s$, $\Delta y = v_2\Delta s$, and $\Delta s = \sqrt{\Delta x^2 + \Delta y^2}$. Because Eqs. (1) and (2) imply that $|\nabla\phi| \neq 0$, the equality in "$\le$" holds if and only if $(v_1,v_2) \,||-\nabla\phi$. In other words, the derivative of $-\phi(x,y)$ in any other direction is smaller than in $-\nabla\phi$. This conclusion is also true regarding the difference quotient of $-\phi(x,y)$ in Eq. (3), provided that Δs is sufficiently small.

Now let the unit vector $(v_1(x,y), v_2(x,y))$ denote the tangent direction of any curve l: $x = x(s)$, $y = y(s)$, that connects (x,y) to some $(x_0,y_0)\in\Gamma_0$, such that $v_1(x(s),y(s)) = dx/ds$, and $v_2(x(s),y(s)) = dy/ds$. We have, by integration of Eq. (3) over the curve,

$$\int_l c\,ds \ge \int_l -\phi_x dx - \phi_y dy = -(\phi(x_0, y_0) - \phi(x, y)) = \phi(x, y), \tag{4}$$

where the second integral is from (x,y) to (x_0,y_0), and the first equality "=" holds because the integral is independent of the path. The first term in Eq. (4) is actually the impedance or accumulated cost over the curve l, and the equality in "$\ge$" holds if and only if $(v_1(x(s),y(s)),v_2(x(s),y(s))) \,||-\nabla\phi((x(s),y(s)))$, or

$$\frac{dx}{ds} = -\frac{\phi_x(x(s), y(s), t)}{\phi(x(s), y(s), t)}, \quad \frac{dy}{ds} = -\frac{\phi_y(x(s), y(s), t)}{\phi(x(s), y(s), t)}, \tag{5}$$

for all (x,y) in l. By setting $x(0) = x_0$, and $y(0) = y_0$, which suggests that $-s$ (other than s) is the arc length between (x_0, y_0) and (x, y), Eq. (5) actually defines a set of characteristics of the eikonal equation, which emit from all $(x_0, y_0) \in \Gamma_0$, and which are able to cover the whole domain.

From the foregoing, we can conclude the following:

(1) $\phi(x,y)$ is the accumulated cost from (x,y) to some $(x_0,y_0) \in \Gamma_0$, over a characteristic defined by Eq. (5), which is smaller than the accumulated cost over any other paths;

(2) For a sufficiently small advancement, $\phi(x,y)$ reduces with the highest rate along the characteristic direction defined by Eq. (5).

The first conclusion means that $\phi(x,y)$ is actually a potential, which can be termed the "cost potential." The upwind scheme used in fast marching (Sethian 1999) and fast sweeping (Zhao 2005)

algorithms for solving the eikonal equation actually follows the inverse direction of Eq. (5), i.e., the advancement of difference in Eq. (2) is from cells with known values (starting from Γ_0 with $\phi(x_0, y_0) = 0$) to those that suggest the highest rate for increase in $\phi(x,y)$. This scheme is in accordance with the second conclusion.

It is possible that characteristics emitting from different points in Γ_0 intersect at some (x,y) (e.g., when the domain includes obstacles or when Γ_0 includes more than one exit for evacuation). In this case, the accumulated costs from (x,y) to Γ_0 over these paths all equal $\phi(x,y)$, and ϕ is continuous. However, ϕ is not differentiable at (x,y), and the set of such (x,y) is usually a discontinuous curve of $-\nabla\phi(x,y)$.

This result is similar to the user-equilibrium condition used in the discrete transportation assignment model, i.e., all selected paths from origin to destination suggest the same accumulated traveling cost, and higher costs would arise for any alternative paths (see, e.g., Lo and Chen 2000; Huang and Lam 2002; Szeto and Wong 2012). However, the points or discontinuous curves with multi-paths in the eikonal equation are trivial for numerical solution, in that numerical errors help smooth the discontinuous profile of $-\nabla\phi(x,y)$ and thus uniquely determine the characteristic directions in all cells.

3.2 Path-Choice Strategy Based on the Potential Field

In the continuum model (Huang et al. 2009; Xia, Wong, and Shu 2009; Jiang et al. 2010; and other papers following this line), the negative gradient $-\nabla\phi(x,y)$ (or Eq. (5)) has been taken as the direction of motion for pedestrians at (x,y). As is indicated, the path suggests only the lowest accumulated cost from (x,y) to Γ_0 at that moment, which is unlikely to be the real cost for these pedestrians traveling to the destination, unless the flow is steady. Therefore, the path choice is actually based on the assumption that these pedestrians anticipate a steady-state flow and thus are able to minimize their traveling costs. Despite its being associated with both the first and second conclusion after Eq. (5), this strategy is just a form of "reactive user equilibrium" or "instantaneous optimization" (Huang et al. 2009). The path-choice strategy used in the discrete dynamic transportation assignment problem can be interpreted similarly.

The negative gradient $-\nabla\phi(x,y)$ can be directly taken as the direction of motion in the continuum model because the amount of pedestrian flow into the pointed cell can be well controlled by the discretized scheme of the flow equation (Huang et al. 2009; Xia, Wong, and Shu 2009; Jiang et al. 2010). The path-choice strategy for the discussed CA model is also based on the potential field. However, $-\nabla\phi$ cannot be directly taken as the direction of motion because it might point to a non-candidate cell, to which a whole individual's movement is forbidden according to the basic rule for occupation. Therefore, we assume that the central part of a pedestrian at (0,0) may move to a candidate cell only if

(1) the motion somehow brings about a reduction in the pedestrian's potential; and

(2) the rate of reduction is not lower than for moving to any other candidate cell.

The path-choice strategy is associated with the second conclusion more than the first one after Eq. (5), and candidate cells satisfying the given conditions are called target cells. The set of such cells is denoted by S_t.

Because the movement of a pedestrian's central part from (0,0) to a neighboring cell (i,j) also brings about the movements of his/her eight controlled parts along the same direction, we take into account the average of nine differential quotients:

$$\bar{q}(i,j) = \frac{1}{9}\sum_{(\xi,\eta)} \frac{\phi(\xi,\eta) - \phi(\xi+i,\eta+j)}{\sqrt{i^2+j^2}}, \tag{6}$$

where (ξ,η) is taken over all nine occupied cells at that moment. Eq. (6) measures the reduction in a pedestrian's potential for moving a unit distance.

We define the set of target cells as $S_t = \{(i,j) \mid (i,j) \in S_c, \bar{q}(i,j) = \bar{q}_M\}$, where $\bar{q}_M = \max_{(i,j)\in S_c}\{\bar{q}(i,j)\}$. Let $\bar{c} = \sum_{\xi,\eta} c(\xi,\eta)/9$, where the average $\bar{c}$ of Eq. (1) is over the nine occupied cells. Approximately, $\bar{c}$ reflects the maximal reduction in potential ϕ for moving a unit distance along $-\bar{\nabla}\phi \equiv -\sum_{\xi,\eta}\nabla\phi(\xi,\eta)/9$, and $\bar{c}_d = \bar{c} - \bar{q}_M \geq 0$, which reflects the deviation of direction

from $-\bar{\nabla}\phi$ for moving to the referred target cell. The probability P_{ij} of moving to a certain target cell $(i,j) \in S_t$ depends on $\bar{c}_d$, $\bar{c}$, and $|S_t|$, where $|S_t|$ is the number of cells in S_t.

In general, we assume that (i) P_{ij} is decreasing if $\bar{c}_d \geq 0$; (ii) $P_{ij} = 0$ if $|S_t| = 0$; and (iii) P_{ij} is shared by all target cells if $|S_t| > 1$. In particular, we discuss the case for $\bar{c}_d = 0$, and $|S_t| = 1$. If there are no other pedestrians in a sufficiently large area between a pedestrian and the destination, then a pedestrian should move almost with $P_{ij} = 1$. In this case, the density ρ in the area is so small on average that $\bar{c}$ will nearly reach its minimum $\bar{c}_{\min} \approx 1$, according to Eqs. (1) and (2). Otherwise, the pedestrian's discomfort or extra cost is measured by $\bar{c} - \bar{c}_{\min} \approx \bar{c} - 1 > 0$, as is the pedestrian's willingness or probability of movement. Thus, we assume that $P_{ij} = 1$, for $\bar{c} = 1$, and that P_{ij} decreases when $\bar{c} - 1$ or $\bar{c}$ increases. The maximum $\bar{c}_{\max}$ of $\bar{c}$ is easily derived from Eq. (2) by setting $\rho = \rho_{max}$ in Eq. (1), which shows that $\bar{c}_{\max} = 1 + g(\rho_{\max})$. Similarly, we know that $\bar{q}_M \in (-\bar{c}_{\max}, \bar{c}_{\max})$.

In summary, we first define a function as follows:

$$P(\bar{c}_d, \bar{c}) \geq 0, P(0,1) = 1, \frac{\partial P}{\partial \bar{c}_d} < 0, \frac{\partial P}{\partial \bar{c}} < 0, \bar{c}_d \in [0, 2\bar{c}_{\max}), \bar{c} \in [1, \bar{c}_{\max}],$$

and then assume that

$$P_{i,j} = \begin{cases} 0, & \text{if } |S_t| = 0, \\ P(\bar{c}_d, \bar{c}) / |S_t|, & \text{otherwise.} \end{cases} \tag{7}$$

In the numerical simulation, we set

$$P(\bar{c}_d, \bar{c}) = \exp(-\gamma_1 \sqrt{\max(\bar{c}_d, 0)} - \gamma_2 \sqrt{\bar{c} - 1}). \tag{8}$$

We note that the probability of Eq. (8) should be decreasing when the average density or the crowdedness in the surroundings increases. The conclusion is correct for $\bar{c}_d = 0$, and is roughly true in general, according to the definitions of $\bar{c}$ and $\bar{c}_d$. This reasonably helps control the frequency of a pedestrian movement that is always at the maximal speed (1 m/s), and implies a negative correlation between the pedestrian's average speed over a period and an average density over the path. The correlation is analogous to the speed–density relationship explicitly applied in the continuum model, which (together with a stable scheme) properly controls the amount of pedestrian flow into the referred cell.

The occurrence of $|S_t| > 1$ is similar to that in the discrete transportation assignment model, in which case the user-equilibrium conditions suggest that the traffic demand be equally divided by some "$|S_t|$" (the precise number of paths) for traveling to the destination. However, a pedestrian cannot be divided into parts that concurrent move to all the cells of S_t. Therefore, we assume that all target cells equally share the probability $P(\bar{c}_d, \bar{c})$ of being occupied.

Combining the foregoing discussion with the discussion in Section 2, we can summarize the rule for updating all pedestrians' positions as follows:

(1) Begin by randomly assigning the positions of $K(0)$ pedestrians in the walking domain at $t = 0$, and/or setting the flow rate or the entering probability of a pedestrian at the entrance;

(2) For time steps $n = 1, \ldots, N$, randomly arrange $K(n)$ pedestrians in a sequence, and for $k = 1, \cdots, K(n)$, the central part of the k-th pedestrian at (0,0) moves to each of the target cells with a probability given by Eq. (7).

3.3 Reconstruction of Densities

The preceding update rule involves the potentials in all inner and semi-artificial cells that can be occupied by pedestrians. For numerical solution of the potentials in Eq. (2), the densities in all these cells should be reconstructed according to the distribution of pedestrians at that moment. The reconstructed density $\rho(x,y)$ should measure the crowdedness of the surroundings, reflect the wall effect, and be as close to the testing data as possible. However, it is unnecessary to obey mass conservation.

We take $\rho(x,y)$ as a weighted average over the cells within a square $A(x,y)$, which is centered at (x, y), contains $(2N_s-1)^2$ refined cells, and has the area $|A| = (2N_s-1)^2 s$, where $s = 0.16/9$ m^2 is the area of a cell. Let $n_p(\xi,\eta)$ be the number of pedestrians in the cell (ξ,η), (e.g., n_p = 1/9, 2/9, 4/9, as shown in Figures 1(a) and (b)), $r(\xi,\eta)$ be the Euclidean distance between (ξ,η) and (x,y), and $w(r(\xi,\eta))$ be the weight regarding the cell (ξ,η). Then, the formula reads

$$\rho(x,y) = \sum_{(\xi,\eta)\in A(x,y)} \frac{w(r(\xi,\eta))n_p(\xi,\eta)}{s}, \quad \sum_{(\xi,\eta)\in A(x,y)} w(r(\xi,\eta)) = 1, \tag{9}$$

and we set $N_s = 4$ in the simulation.

For the application of Eq. (9), at most N_s artificial cells are extended to the outside. Pedestrians tend to keep their distance from walls. In addition, a pedestrian near a wall is very likely to be compressed or pushed by others in overcrowded situations, so that he/she has to be tangent to the wall. To reflect both characteristics, we suppose that an artificial cell and the half of a semi-artificial cell within the wall are "occupied" by n_a and $n_a/2$ pedestrians, respectively, such that the "average density" outside the domain is around the maximum $\rho_{\max}$ = 14.06 ped/m^2. Thus, we assume $n_a = s\rho_{\max}$ = 0.25 ped; n_a could also be adjusted according to numerical simulations, experiments, and/or further analyses.

Eq. (9) reduces to a simple average if the weights are all set to be $w(r(\xi,\eta)) \equiv (2N_s\text{-}1)^{-1}$. However, it is reasonable that the weight $w(r)$ decreases according to r. Thus, we assume

$$w(r(\xi,\eta)) = \frac{\exp(-r^2(\xi,\eta)/R^2)}{\sum_{(\xi,\eta)\in A(x,y)} \exp(-r^2(\xi,\eta)/R^2)}, \quad R = \max_{(\xi,\eta)\in A(x,y)} \{r(\xi,\eta)\},$$

which is modified from a commonly adopted measurement (e.g., see Helbing, Johansson, and Al-Abideen 2007). The formulation is also a revision of that in Zhang et al. (2012), which adopted a simple average and did not consider the wall effect.

3.4 Extension to Model Two Pedestrian Groups

Pedestrian groups a and b in the same walking domain are distinguished by their destinations Γ_a and Γ_b. Then, all rules and assumptions are the same as in the foregoing discussion, except that

(1) Two potential fields $\phi_a(x,y)$ and $\phi_b(x,y)$ are established by setting $\phi_a(x,y) = 0$, for $(x,y)\in\Gamma_a$, and $\phi_b(x, y) = 0$, for $(x,y)\in\Gamma_b$, respectively; and

(2) The cost distribution $\tau_c(x,y)$ of pedestrian group c ($c = a$ or b) is magnified by $L^c \geq 1$, which reflects stronger interaction between the two pedestrian groups.

More precisely, we define

$$\tau^c(x,y) = C(\rho(x,y))L^c(\psi,\rho^d), \quad (c,d) = (a,b) \text{ or } (b,a), \tag{10}$$

where the densities ρ and ρ^c reflect the crowdedness respectively for all pedestrians in general and for pedestrian group c in particular. The intersecting angle between the streamlines of two pedestrian groups at (x,y) is defined by

$$\psi(x,y) = <-\nabla\phi^a(x,y), -\nabla\phi^b(x,y)>, \quad 0 \leq \psi \leq \pi. \tag{11}$$

For $\psi > 0$, $\rho^d > 0$ (with $L^c > 1$) should suggest stronger discomfort or more cost than $\rho^d = 0$ (with $L^c = 1$) because mingling is only among the same group in the latter case. Similarly, for $\rho^d > 0$, $\psi > 0$ (with $L^c > 1$) suggests stronger discomfort or more cost than $\psi = 0$ (with $L^c = 1$) because the two groups are viewed as being identical (locally at (x,y)) in the latter case. The arguments imply the following properties of the function $L^c(\psi, \rho^d)$:

- **Monotonicity**: L^c increases according to ψ and ρ^d, for $\rho^d > 0$ and $\psi > 0$, respectively; and
- **Consistency**: $L^c(0, \rho^d) = L^c(\phi, 0) \equiv 1$.

The formulation for two pedestrian groups should exactly reduce to that for one pedestrian group, provided that (i) the destinations Γ_a and Γ_b are identical, or (ii) pedestrian group a (or b) vanishes all over the simulation in the walking domain. This strong consistency is guaranteed if ρ and ρ^c are properly reconstructed and the initial values of ψ are properly given, as in the following. We reconstruct the "total density" ρ by taking into account the distribution of all pedestrians and the wall effect in Eq. (9). However, ρ^c is reconstructed such that n_p only counts in the pedestrians of group c, without consideration of the wall effect. At time step n, $\psi(x,y,n)$ used in Eq. (10) is approximated by $\psi(x,y,n\text{-}1)$ at time step $t = n\text{-}1$; initially, $\psi(x,y,\text{-}1)$ is derived through Eq. (11) by setting $L^c \equiv 1$ in Eq.

(10).

The formulation is similar to that in Xiong et al. (2011), and Zhang et al. (2012) (and other studies dealing with similar problems). However, strong consistency was not guaranteed in these works. Thus, our study extends these related works.

4. SIMULATION

The discomfort measured by $g(\rho)$ in Eq. (1) is given by

$$g(\rho) = \alpha(\rho / \rho_c)^{\gamma},\ \rho_c = 6.25\text{ped}/\text{m}^2,\ \gamma > 1, \tag{12}$$

where the parameter $\alpha \equiv g(\rho_c)$, significantly measures the discomfort at the critical density $\rho = \rho_c$, and the non-dimensional parameter γ reflects the increasing rate of $g(\rho)$. Referring to a field study (Wong et al. 2010) and numerical experiments (Xiong et al. 2011; Zhang et al. 2012), we set the magnifier in Eq. (10) as

$$L^c(\psi, \rho^d) = \exp(\beta(1-\cos\psi)(\rho^d / \rho_m)^2), \tag{13}$$

where the non-dimensional parameter β reflects the magnitude of L^c. In the following simulations, we take $\alpha = 0.2$, and $\gamma = 4.0$.

4.1 Fundamental Diagram

Initially, N pedestrians are randomly distributed in a 10 m × 10 m corridor divided into 75 × 75 cells. It is assumed that the top and bottom boundaries are solid, and that the right boundary is the destination. See Section 2.1 for the division of a domain by cells. The boundary conditions are assumed to be periodic; namely, those arriving at the right boundary immediately enter the corridor from the left boundary. Therefore, the number N of pedestrians remains unchanged in the simulation, and the average density N/100 m^2 in the corridor also remains constant. After time t, when the flow state becomes relatively stable, we begin to record the number of pedestrians crossing an arbitrary line perpendicular to the solid boundaries, until time $t+T$. In this way, we derive the average flow rate over the period $[t, t+T]$.

We set t = 533.33 s (4000 time steps), T = 133.33s (1000 time steps), and the line for flow recording at 2 m away from the destination. To depict the flow–density relationship (the fundamental diagram), we vary the number of pedestrians by setting N = 50, 100, …, 1400. Figure 4 shows these simulated fundamental diagrams using a variety of parameter values for γ_1 and γ_2 in Eq. (8). We note that $\gamma_1 = \gamma_2 = 2.0$ suggests a fundamental diagram that agrees well with the one derived from the field study in Helbing, Johansson, and Al-Abideen (2007); these values are therefore applied in the following simulations. Figure 4 also indicates that the fundamental diagram is more sensitive to change in γ_2 than in γ_1.

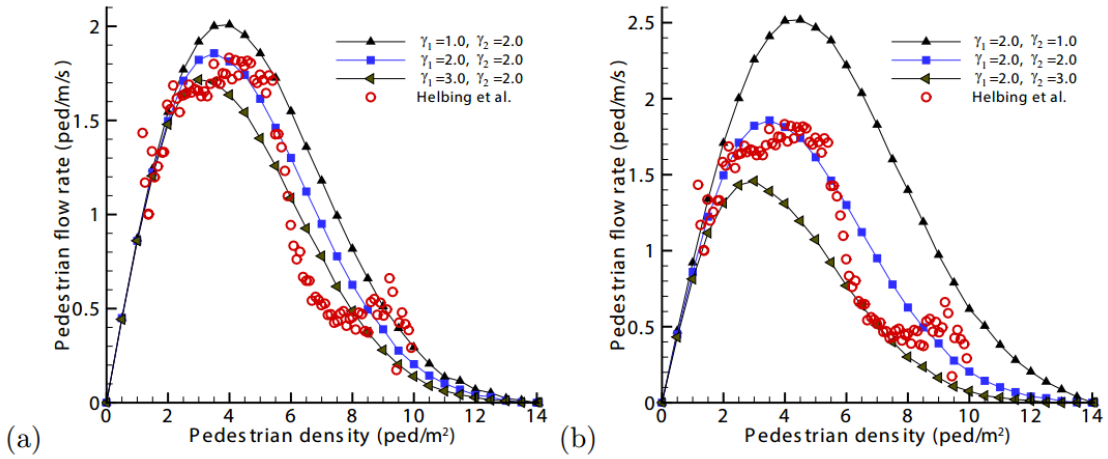

Figure 4. Fundamental diagrams compared with the one in Helbing, Johansson, and Al-Abideen (2007). (a) With γ_2 fixed, the capacity (the maximal flow rate) increases with γ_1; (b) with γ_1 fixed, the capacity (the maximal flow rate) increases with γ_2. The results show that $\gamma_1 = \gamma_2 = 2.0$ is appropriate, and that the fundamental diagram is more sensitive to change in γ_2.

For comparison with the so-called potential field (PF) model (Zhang et al. 2012) and perceived potential field (PPF) model (Jian et al. 2014), we implement similar simulations to find proper parameter values that are fitted to the observed fundamental diagram (Helbing et al. 2007). Under the normal visibility condition, changes in the simulated fundamental diagrams by the PPF or PF model mainly arise from changes in the cost distribution. Moreover, the PPF model is an extension of the PF model, i.e., the two models are equivalent for a density not greater than 6.25 ped/m^2, which is the maximal density in the PF model. Therefore, we can still apply Eq. (12) to the two models, and we try to find those α and γ that are most fitted for $\rho < 6.25$ ped/m^2.

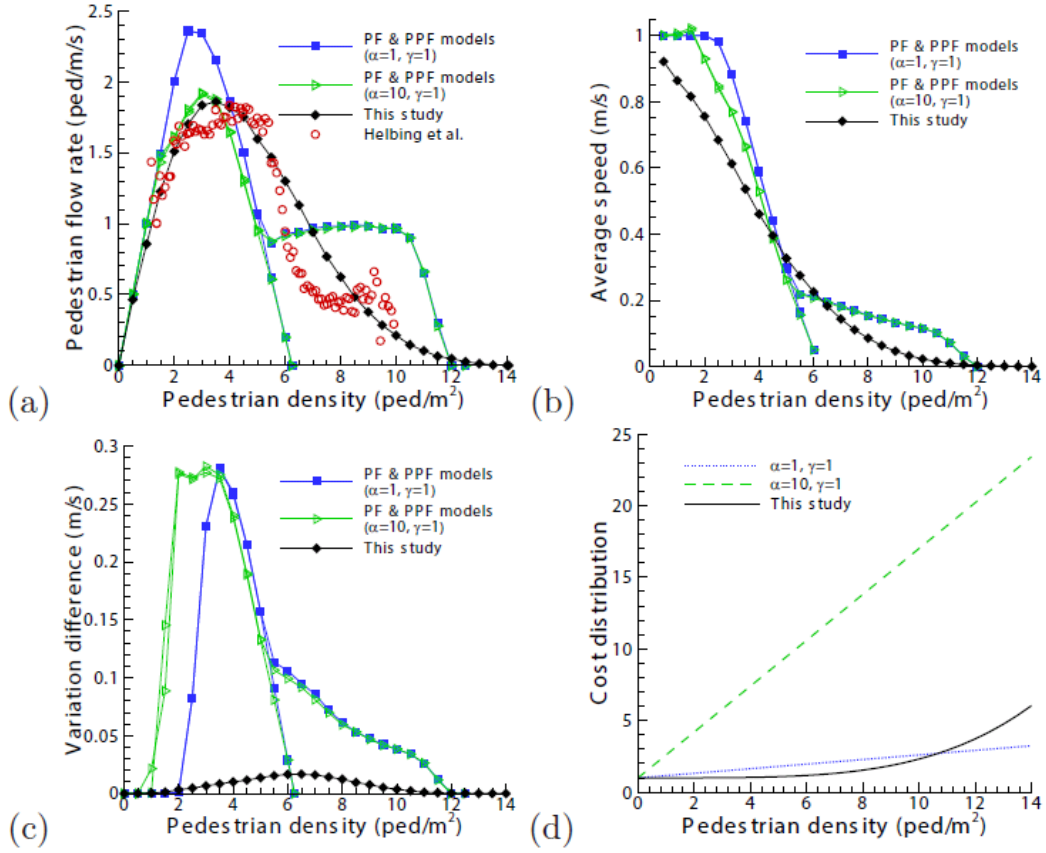

Figure 5. Comparison of the PF, PPF and proposed models, (a) fundamental diagrams; (b) speed–density relationships; (c) variational differences in vertical displacement; (d) cost distributions. The results show that the PF and PPF models unreasonably suggest much larger speeds than the proposed model. Therefore, they should increase the costs and suffer more detours to reduce the flow rates or accommodate to the observed fundamental diagram in a density region much smaller than 6.25 ped/m^2. However, the PPF model reproduces unrealistic flow rates in the other density regions.

Figure 5(a) shows a fundamental diagram for $\alpha = 10$, and $\gamma = 1$, which appears to agree with the observation in the aforementioned density region. However, our experiments cannot help us find any α and γ that are even just "apparently" suited in the whole density region. This raises doubts about the PPF model for its introduction of an aggregate force for $\rho > 6.25$ ped/m^2, which corresponds to too high flow rates in Figure 5(a). Here and hereafter, we also show the results with $\alpha = 1$ and $\gamma = 1$, to observe the influence of cost distribution on the PF or PPF model.

For the density region $\rho \leq 6.25$ ped/m^2, which is the main concern in the following, one major difference of the PF and PPF model from the present work is that we introduce a smaller probability for a pedestrian's moving to a target cell (Eqs. (7) and (8)). In contrast, a target cell would surely be occupied by a pedestrian even under crowded conditions according to the PF or PPF model. This generally suggests a higher speed–density relationship in the PF or PPF model than that in the proposed model, even though the parameter α is adjusted to fitting the observed fundamental diagram (flow–density relationship) in the PF or PPF model.

Figure 5(b) shows the speed–density relationships by implementing the same simulation as above,

where the speed is the average over all pedestrians and the interval [533.6 s, 666.8 s]. With a suitable parameter α = 10, the PF and PPF models do not show higher flow rates than the proposed model (Figure 5(a)); however, they show much higher speeds than the proposed model (also with α = 1) (Figure 5(b)). The explanation can only be that the PF and PPF model suggest more detours than the proposed model. The degree of detours for the α-th pedestrian can be measured by the variational difference (*VD*) of $y_\alpha(t)$, where y_α (t) is the vertical displacement at time *t*. The average *VD* over all *N* pedestrians and the interval [*t*, *t* +*T*] can be computed by the following

$$VD_y = \frac{1}{NT}\sum_\alpha \sum_n |y_\alpha(t_{n+1}) - y_\alpha(t_n)| \approx \frac{1}{N}\sum_\alpha \frac{1}{T}\int_t^{t+T} |y'(t)|dt,$$

where the increment $\Delta t \equiv t_{n+1} - t_n$ = 0.4 s. The last expression shows that VD_y also denotes the average speed in the vertical direction over all pedestrians and the interval. Figure 5(c) shows the curves $VD_y = VD_y(\rho)$, which indicates that the PF or PPF model unreasonably reproduces much larger *VD* or average speed in vertical directions than the proposed model does.

The degree of detours seems to be related to the cost distributions (Figure 5(d)). For the PF and PPF model, a comparison of Figures 5(a), (c) and (d) indicates that more costs result in more detours and lower flow rates for approximately ρ < 3 ped/m^2. For ρ > 3 ped/m^2, both detour and flow rates mildly decrease with the increase of the costs. Here, 3 ped/m^2 is very close to the critical density that corresponds to the maximal flow rate. Figure 5(b) shows that the average speed decreases with the increase of the cost approximately for ρ > 2 ped/m^2, which agrees with the aforementioned comparison.

4.2 Evacuation with One Exit

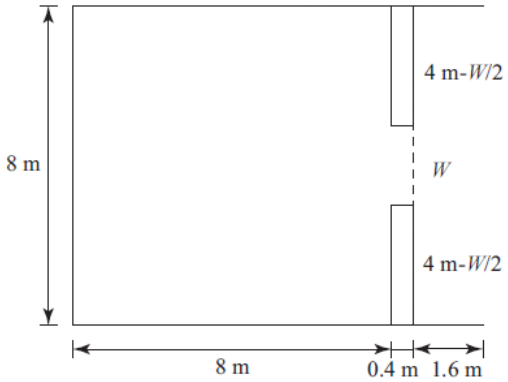

Figure 6. Layout of the room with one exit: the destination and right boundary is set outside and 1.6 meters away from the exit.

We simulate evacuation from an 8 m × 8 m room with one exit, where an outside vertical line is set as the destination and the right boundary. The layout is shown in Figure 6. Initially, *N* pedestrians are randomly distributed in the room. Figure 7 shows the simulation results, with *N* = 400, and the width of door *W* = 1.6 m. In the evacuation process, we observe the so-called “arching phenomenon” near the door.

To study the influence of the number of pedestrians and the width of the exit on evacuation, two sets of simulation experiments are implemented. With *N* being fixed, we vary the width *W* of the exit by setting *W* = 0.4, 0.8, ..., 4 m; moreover, we set *W* = 0.53, 0.67, 0.93, 1.07, 1.33, 1.47 m in the experiment for comparison with other results in the literature.

Figure 8(a) shows the relationships between *W* and evacuation time, by which we see that the evacuation time dramatically increases as *W* decreases approximately from *W* = 1.5 m, especially when *N* is large. As *W* increases from *W* = 1.5 m, the evacuation time decreases slightly, especially when *N* is small (e.g., for *N* = 100). In the latter case, the last pedestrian is able to evacuate from the room almost unimpeded by anyone in front of him/her. These results are in accordance with common sense. Next, with *W* fixed, we vary *N* by setting *N* = 50, 100, ..., 900. Figure 8(b) shows the relationship between *N* and evacuation time, which approximately suggests a linear function for each value of *W* given in the figure. For each pair of values of *N* and *W*, we note the evacuation time as an

average from repeating the simulation 10 times. The other quantities in the following discussion are derived similarly.

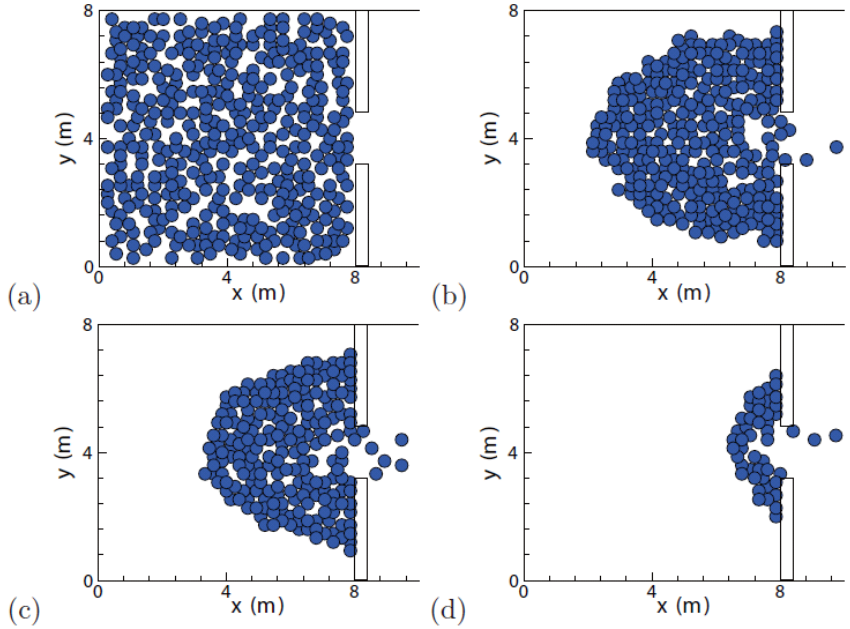

Figure 7. Evacuation process, N = 400, W = 1.6 m, (a) t = 0 s; (b) t = 40 s; (c) t = 80 s; (d) t = 148 s.

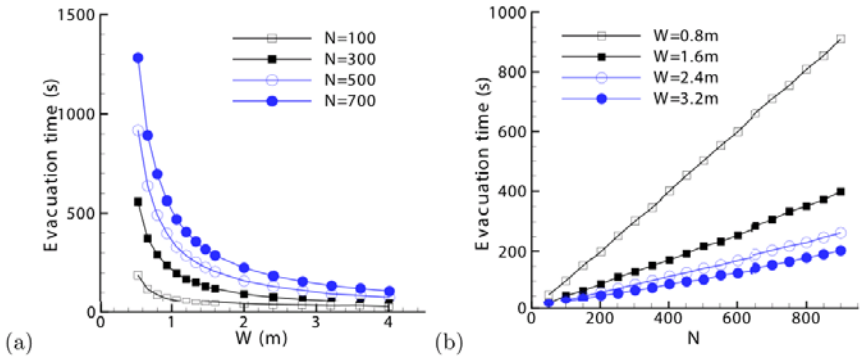

Figure 8. Relationships between the evacuation time and (a) the width of the exit (*W*); (b) the number of pedestrians (*N*).

In the evacuation process, the average flow *n*/10 s at the exit is recorded every 10 s, where *n* is the number of pedestrians passing through the exit in the interval. The maximum n_{max}/10 s can be viewed as the capacity at the exit, and its relationship with the width of the exit is shown in Figure 9(a). The relationship between the maximal flow rate n_{max}/W/10 s and the width *W* is also shown in Figure 9(b). These results agree well with those in Kretz, Grünebohm, and Schreckenberg (2006), Seyfried et al. (2009), and Müller (1981).

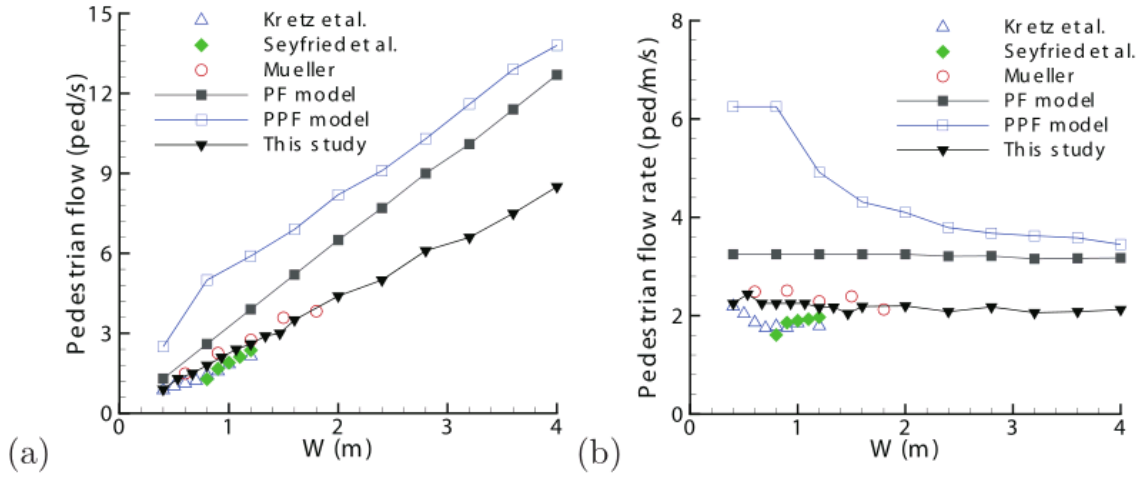

Figure 9. Maximal flows (a) and flow rates (b) for evacuation at the exit, as the width of exit varies. Because there are hardly any detours for pedestrians going through the exit, the capacities reproduced by the proposed model are somewhat larger than that in Figure 5(a), and agree well with those in the literature; the capacities reproduced by the PF and PPF model are much larger than that in Figure 5(a).

The simulated maximal flow rates or capacities are around 2.2 ped/m/s in Figure 9(b), which is somewhat greater than the maximum 1.85 ped/m/s that approximately corresponds to $\beta = 3.75$ in Figure 5(a). This difference should mainly be associated with a large degree of detour or vertical movement in reproducing the latter flow rates. In contrast, the former flow rates are recorded by counting flow-out through the exit, in which case there would hardly be any detours or vertical movements. Such a difference together with the explanation can be more clearly indicated by the simulated results using the PF or PPF model. With $\alpha = 10$, and $\gamma = 1$, the capacity is around 1.9 ped/m/s in Figure 5(a), but equals or is much greater than 3.2 ped/m/s in Figure 9(b).

4.3 Lane Formation in Pedestrian Counter-Flow

Assume a 24 m × 8 m corridor. Initially, the corridor is empty and two pedestrian groups begin to enter the corridor from the left (group I) and right (group II) boundaries, which are set as the destinations of groups II and I, respectively. Pedestrians cease entering as long as the total number N of pedestrians in the corridor is at least a given value of N. Then, the periodic boundary conditions are adopted.

For $N = 400$, we assume that 10 pedestrians of each group enter the corridor every 1.2 s at the beginning, by randomly occupying 10 of the 60 cells adjacent to the entrance. Thus, the inflow rate equals 1.04 ped/m/s, and the average density in the corridor eventually reaches 2.08 ped/m^2. Figure 10 shows three snapshots of the movement. We clearly observe the approach of two pedestrian groups at $t = 13.33$ s (Figure 10(a)), their segregation at $t = 40$ s (Figure 10(b)), and the formation of lanes at $t = 66.67$ s (Figure 10(c)).

The simulated lane formations in counter-flow can be ascribed to Eqs. (10) and (13), which enlarge the costs for any pedestrians to mingle with the other group. To minimize the costs, the head pedestrians of the two groups try to avoid direct confrontation as they approach each other, and other pedestrians follow the lead pedestrians of their groups. See Xiong et al. (2011) and Zhang et al. (2012) for detailed discussions of a similar mechanism. The enlarged cost or discomfort in Eq. (13) is reflected by the parameter β. By repeating the experiment 100 times, with $t \leq 266.67$ s, and $\beta = 0$, 0.1, …, 1, Figure 11(a) shows the probabilities of gridlock corresponding to β. Here, gridlock is defined such that no more than four pedestrians are able to cross the central line ($x = 12$ m) in the final 6.67 s (50 time steps). The probability is decreasing when β increases, and we find no gridlock for β being sufficiently large.

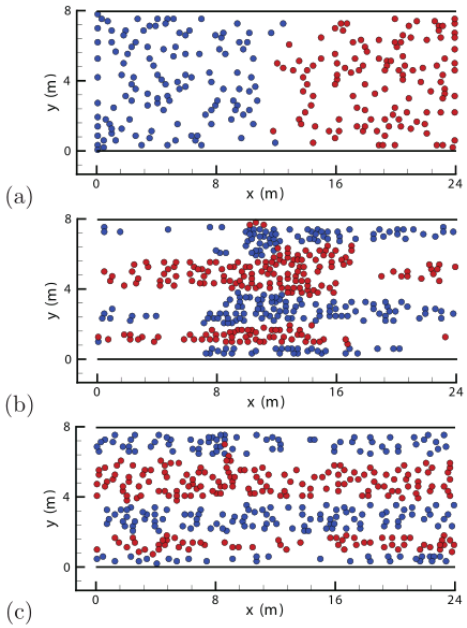

Figure 10. Formation of lanes in counter-flow, for total number $N = 400$ of pedestrians in the corridor, with $\beta = 3.75$. Snapshots at (a) t = 13.33 s; (b) t = 40 s; and (c) t = 66.67 s.

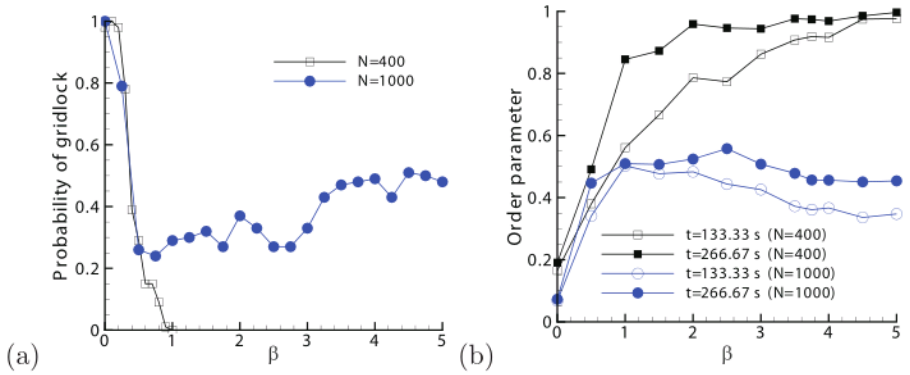

Figure 11. (a) The probability of gridlock, and (b) the order parameter, which are associated with the parameter β in Eq. (13). For $N = 400$, or $N = 1000$, and $\beta < 1$, a larger β suggests larger discomfort for pedestrians of one group mingling with those of the other group, and thus a smaller probability of gridlock and higher degree of order. However, for $N = 1000$, and β that is larger, the increase in β does not help reduce the probability of gridlock or increase the degree of order.

We also study the "degree of order" using an order parameter defined as follows (Nowak and Schadschneide 2012):

$$\omega = \frac{1}{N}\sum_{\alpha=1}^{N}\omega_\alpha, \qquad \omega_\alpha = \left(\frac{N^{\mathrm{I}}_{j_\alpha} - N^{\mathrm{II}}_{j_\alpha}}{N^{\mathrm{I}}_{j_\alpha} + N^{\mathrm{II}}_{j_\alpha}}\right)^2,$$

where $N^{\mathrm{I}}_{j_\alpha}$ ($N^{\mathrm{II}}_{j_\alpha}$) is the number of pedestrians in the same line with the α-th pedestrian, belonging to group I (II). It is easy to see that $\omega \le 1$, and the equality holds if and only if $N^{\mathrm{I}}_{j_\alpha} = 0$, or $N^{\mathrm{II}}_{j_\alpha} = 0$, for all α, which denotes the highest degree of order or lane formation. Figure 11(b) shows the order parameter for changes of β in a wider range, corresponding to certain times in the simulation. For a certain time t, the order parameter ω is roughly an increasing function of β. When β is fixed, the pedestrians in counter-flow enjoy a higher degree of order for a larger simulated time.

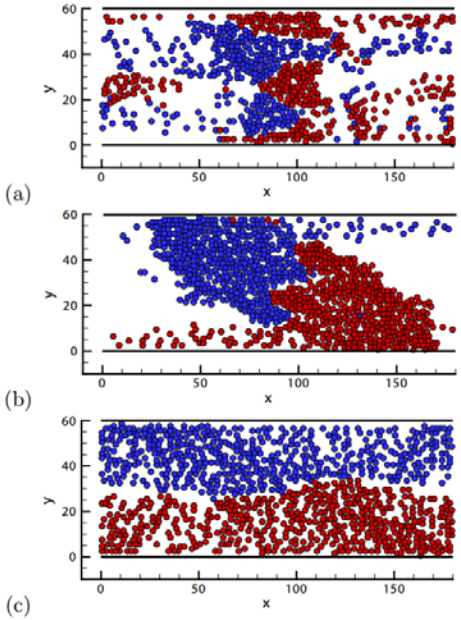

Figure 12. Formation of lanes in counter-flow, for total number N = 1000 of pedestrians in the corridor. (a) t = 80 s; (b) t = 240 s; (c) t = 480 s.

We reset N = 1000 and implement a similar simulation, which is described in the following. Assume the same inflow rate as for N = 400 before the total number of pedestrians reaches 320 in the corridor. Then, the inflow rate becomes smaller such that only 5 pedestrians from each group enter the corridor every 1.2 s until the total number of pedestrians reaches 660. Thereafter, we assume the entrance of two pedestrians for each group in the same interval. Intuitively, the probability of gridlock (and the order parameter) should increasingly (decreasingly) depend on the average density or total number N of pedestrians in the corridor. With β = 1, 1.25, …, 4.75, 5, the results are also shown in Figure 11 for comparison. Indeed, we observe a much higher possibility of gridlock (Figure 11) and lower degree of order than for N = 400, particularly when $\beta > 1$. However, it seems that a further increase in β does not help reduce the probability of gridlock and improve the degree of order when N is sufficiently large. On the contrary, Figures 11(a) and (b) respectively show a weakly increasing and decreasing tendency of the curves corresponding to N = 1000, for $\beta > 1$. It seems that too strong a dislike of mingling with the other group does not significantly help improve the efficiency of counter-flow; it even worsens the traveling situation, especially when the density is considerably large. This interpretation seems to be in accordance with common sense. Here, β functions similarly to K_a in the floor field model, which reflects the magnitude of a repulsive force arising from the anticipation field of Nowak and Schadschneide (2012).

Figure 12 shows three snapshots of a simulation for β = 3.75, in which case the pedestrian movement is fortunately free from gridlock with a much smaller probability than that for N = 400 (see also Figure 11(a)). Comparing with Figure 10, we can see more interactions between the two pedestrian groups in the movement (Figures 12(a) and (b)). Moreover, it takes much longer for the two pedestrian groups to segregate themselves completely into two streams. In this case, the average density in the corridor eventually reaches 5.21 ped/m^2, which falls into the danger zone for a complete blockage or even an accident. The formation of lanes is essentially related to the numerical viscosities in solving the eikonal equation, which is somehow “biased” and helpful to the segregation of two pedestrian groups in counter-flow. Otherwise, we should have observed direct confrontation at the first meeting of the two pedestrian groups, and then a complete blockage. Theoretically, this is obviously true for the (deterministic) continuum model (Xiong et al. 2011). Figure 12(a) shows that each flow is approximately symmetric to the central line y = 4 m. However, we find more pedestrians of group I (II) traveling above (below) the central line, which indicates that pedestrians in groups I and II have tendencies of turning to the upper right and lower left respectively in the mingling. These biased tendencies are more clearly reflected in Figure 12(b). As a consequence, the two groups are eventually segregated roughly by the central line y = 8 m (Figure 12(c)).

The biased numerical viscosity significantly influences the collective behavior of multi-group pedestrian flows, which will be studied in depth in the future. Under the influence of the aforementioned tendencies, microscopic performances of five pedestrians in each group in Figure 12 are observed, and Figure 13 shows their trajectories for $t \leq 480$ s, which are expanded to travel through four spatial domains under periodic boundary conditions. All of these pedestrians enter domain A after one time step (0.1333 s). For reference, the times for their entering the other three domains are shown in Table 1; the average speeds over each of the first three domains are shown in Table 2. Here and hereafter, the average speed refers to the horizontal direction.

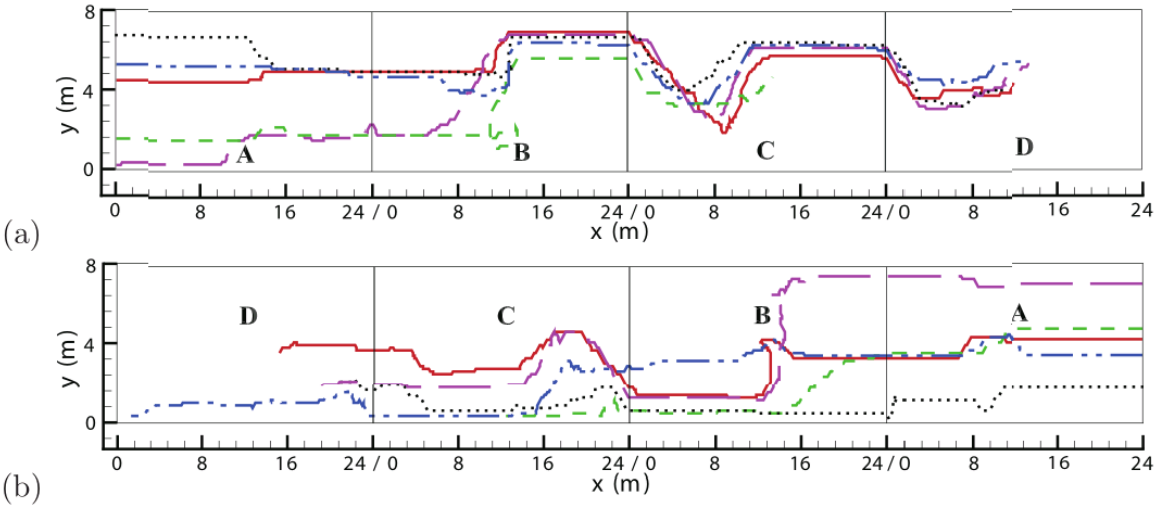

Figure 13. Trajectories of five pedestrians (a) in group I and (b) in group II, which are expanded to travel through four spatial domains A, B, C, and D, under periodic boundary conditions for $t \leq 480$ s. The five pedestrians in group I (II) are sequenced from the top (bottom) to the bottom (top) at their start from the left (right) boundary to the right (left), and labeled by I*l* (II*l*) for $l = 1, ..., 5$. The trajectories are shown by black (dotted), blue (dash dot dot), red (solid), green (dashed), and purple (long dash) colors (curves) following the sequence.

Table 1. Times for pedestrians entering domains B, C and D (unit: s), referring to Figure 13

	Group I					Group II				
	1	2	3	4	5	1	2	3	4	5
B	39	37	42	36	67	79	37	36	84	40
C	249	288	177	399	244	284	93	311	250	315
D	415	408	418		384	462	283	448		458

Table 2. Average speeds of pedestrians in the horizontal direction across domains A, B and C (unit: m/s), referring to Figure 13

	Group I					Group II				
	1	2	3	4	5	1	2	3	4	5
A	0.61	0.65	0.57	0.67	0.36	0.30	0.64	0.67	0.29	0.60
B	0.11	0.10	0.18	0.07	0.14	0.12	0.43	0.09	0.14	0.09
C	0.15	0.20	0.10		0.17	0.14	0.13	0.18		0.17

Pedestrian I4 is the first in his/her group to enter domain B, followed by pedestrians I2, I1, and I3 with almost the same average speed over domain A. Note that there have been 460 pedestrians in the corridor until $t = 36$ s. However, pedestrian I5 takes much longer to arrive at domain B with a much lower average speed over domain A, which indicates that he/she has encountered a crowd of pedestrians from group II. Pedestrians II1 and II4 take even longer to arrive at the domain, and can be positioned somewhere near the coordinates (24 m,0 m) and (0 m,4 m) in Figure 12(a), respectively, according to their trajectories and arrival times.

Pedestrian II2 is the first to enter domain C, when the number of pedestrians has reached 772. He/she goes almost straight along the central line $y = 4$ m in domain B (Figure 13(b)) and has

fortunately avoided a confrontation with pedestrians from group I before t = 80 s (Figure 12(a)). Pedestrian I4 becomes the last at t = 398 s, although he/she is the first in his/her group to enter domain B. This indicates that he/she does not escape from the aforementioned confrontation, which becomes even worse with the increase of incoming pedestrians. Pedestrian I4 could be positioned among the lower and middle crowded area in Figure 12(a)), for whom going forward becomes impossible. Therefore, he/she has to move backward and then goes for the upper region almost vertically. This process lasts for so long that he/she should still be among the central crowded region in Figure 12(b) according to his/her trajectory (Figure 13(a)) and arrival time at domain C. Pedestrians II3 and II5 undertake a similar journey and could be positioned in a crowded middle regions in both Figures 12(a) and (b). However, they arrive at domain C much earlier than pedestrian I4, which indicates that they (especially pedestrian II3) should have avoided direct confrontation with pedestrians from group I, according to their trajectories in domain B (Figure 13(b)). Pedestrian II1 keeps to the bottom line without meeting pedestrians from group I, which helps him/her overtake pedestrians II3 and II5. Note that all pedestrians have entered the corridor by t = 161 s.

After entering domain C, the five pedestrians in group I travel toward the lower right (Figure 13(a)) naturally along a sloping edge of the crowded region, which can be observed in Figure 12(b) for t = 240 s. Pedestrian I3 has entered domain C before that, followed by pedestrians I5, I1, I2, and I4 sequentially after t = 240 s. Their positions can be roughly sorted in Figure 12(b). Because the empty spaces in the lower middle area are gradually filled up in the process, the trajectory of pedestrian I3 shows a turning point lower and farther forward than the others. At the turning points, these pedestrians (except pedestrian I4) meet (or are very close to the meeting) the incoming crowd from group II; therefore they turn to the upper right to escape from (or avoid) the confrontation. The escaped pedestrians naturally turn right and form a stream (Figure 13(a)) that is gradually expanded in size (the width and length) by including more and more pedestrians. This maintains a stable density that is not high enough to guarantee a straightforward movement (Figure 13(a)). In the expansion, the stream seems to compete with those pedestrians (like II3 and II5) who appear to occupy the empty upper right area (Figure 12(b)) after their entering domain C from lower positions on the right-hand side (Figure 13(b)). However, most of these pedestrians (like II3 and II5) turn to the lower left midway to join an escape of their group, which similarly takes place in an area near the bottom (Figure 12(b)). Pedestrians I5, I2, I1 and I3 enter domain D sequentially. Then they go toward a lower right empty area (Figure 13(a)). Before that, the two pedestrian groups should have completely segregated without a large-scale confrontation.

The trajectories embody several interesting traveling modes, some of which are summarized in the following, mainly referring to Figure 12 and Table 2. Pedestrian II2 smoothly travels over domain A and is the only one to escape from being outflanked in domain B (Figure 12(a)), which allows him/her to take an earlier turning to the lower left in domain C and then travel all the way along the bottom. Pedestrian I4 is the fastest traveling over domain A, which makes him/her deeply involved in a confrontation in domain B according to his/her lower starting position and trajectory. Pedestrian II4 encounters a jam in domain A. Although he/she obviously overtakes pedestrians II3 and II5 in domain B, he/she again encounters a jam after entering domain C, which makes him/her among the last in his/her group. Consequently, pedestrians I4 and II4 do not enter domain D until the end of the simulation.

5. CONCLUSION

We propose a multi-grid potential field CA model for overcrowded pedestrian flow, which explicitly describes physical contacts among pedestrians. The model not only extends the work in Zhang et al. (2012) by allowing a much larger maximal density, but greatly enhances the spatial and temporal continuity of the models in Zhang et al. (2012) and Jian et al. (2014). Moreover, it significantly improves the updating rules in the aforementioned works by introducing a smaller probability of a pedestrian's movement (Eqs. (7) and (8)). This generally suggests a weaker speed–density relationship (Figure 5(b)) even for lower traveling costs (Figure 5(d)), which helps reduce the number of unreasonable detours. In contrast, the models in Zhang et al. (2012) and Jian et al. (2014) result in much more unrealistic detours (Figure 5(c)) or higher flow rates through an exit (Figure 9), in which case there are hardly any detours. The introduced probability helps control the frequency of

movement that is always at the maximal speed (1 m/s) regardless of the density in the surroundings, and the function is analogous to the speed–density relationship in the continuum model.

Much larger costs due to the dislike for mingling of two pedestrian groups are reasonably introduced in the cost distribution, by which the self-organized lane formation phenomenon is reproduced in pedestrian counter-flow. The numerical results show that moderate dislike for mingling has a negative and positive correlation with the probability of gridlock and the degree of formation of lanes, respectively. However, the correlations are weak when dislike is very strong and even become opposite when the number of pedestrians is considerably large. In this case, the probability of preventing a complete blockage is relatively small, and the trajectories show a long and hard journey for most pedestrians to travel over several periodic domains (Figure 13).

Although not mentioned in the foregoing discussions, the effects of walls and artificial cells can also be observed in the snapshots. Figures 7(b), (c) and (d) show that many semi-artificial cells adjacent to the wall near the exit are occupied by pedestrians as a consequence of their being compressed by others under overcrowded conditions, and similar phenomena can be observed in Figures 10 and 12. The repulsive effects of the wall are also reflected in Figures 10 and 12, which show pedestrians keeping a reasonable distance away from the wall in the movement, subject to relatively smaller densities of the crowd against the wall.

Given its microscopic nature, the proposed model is more suited to the description of pedestrian flow in small- and medium-scale facilities by presenting detailed or animated pictures. This is an advantage over its macroscopic counterpart or the continuum model which adopt a similar path-choice strategy subject to the eikonal equation, but which are more suited to large-scale pedestrian movements due to computational efficiency. Regarding to the computational complexity, the proposed model should be at the same degree as other CA models when adopting the same size of cells. This was shown by Figure 3 in Zhang et al. (2012) through comparison of CPU times between the potential field and floor field models, which adopted the same division by normal cells of size 0.4 m × 0.4 m. In fact, the dynamic field in the floor field model is essentially acquired from a partial differential equation modeling the diffusion and decay of a pedestrian's trace, which should not save more computational resources than the eikonal equation for numerical solution. However, the CPU time used by the proposed model should be roughly nine times that for the same number of pedestrians in the same walking domain because the cell and update times are three times smaller. This would also be the case for a floor field model extended by similar refinement.

The proposed model should have an advantage over other microscopic CA models mainly because of its path-choice strategy. First, it is more suited to walking domains with complex geometry because the searching of paths can automatically keep away from walls or obstacles. Moreover, all exits can be viewed as one destination for evacuation, in which case we need to deal with only a group of pedestrians. Second, it is more suited to the navigation of evacuation from a calamity (e.g., an earthquake, conflagration, etc.) by timely and conveniently incorporating any adverse influences on the path in the cost distribution, e.g., by assigning infinitely great values to Eq. (1) in burning or smoke-filled areas. Third, its optimal path-choice strategy is straightforward to help with the design or improvement of a walking facility. These are promising applications. Some theoretical shortcomings or problems of the model are listed below for follow-up in future studies.

(1) Isotropic movement should be considered by forbidding diagonal movements and using refined square cells of smaller size, or by considering refined hexagonal cells.

(2) The function L being consistent with Eq. (10) should be extended to reflect interactions among pedestrians of more than two pedestrian groups. For this purpose, we refer the reader to Xie and Wong (2015), Hussein and Sayed (2017), and Kielar et al. (2018).

(3) The biased numerical viscosities mentioned in Section 4.3 could be clearly indicated through analysis of the numerical schemes, as is the influence on the evolution of two (or even more) pedestrian groups.

(4) The path-choice strategy could possibly be extended to describe crowds in panic (or other adverse situations) under the current framework, e.g., by assuming a disturbed recognition of finding the "optimal" direction of motion and resetting the parameters in Eqs. (7) and (8) such that the recognition and the probability of movement differ between individuals and from time to time.

ACKNOWLEDGMENTS

This study was jointly supported by grants from the National Natural Science Foundation of China (Grant Nos. 11672348, 71531011, 11272199), the Research Grants Council of the Hong Kong Special Administrative Region, China (Grant No. 17201318), the National Basic Research Program of China (Grant No. 2012CB725404), the Science and Technology Innovation Program of the Department of Transportation, Yunnan Province, China (Grant No. 2019303), and the Opening Research Fund of National Engineering Laboratory for Surface Transportation Weather Impacts Prevention (Grant No. NEL-2019-03).

REFERENCES

Burstedde, C., K. Klauck, A. Schadschneider, and J. Zittartz. 2001. "Simulation of pedestrian dynamics using a two-dimensional cellular automaton." *Physica A: Statistical Mechanics and Its Applications*, 295 (3-4): 507-525.

Chen, M., D. Han, and H. Zhang. 2011. "Research on a multi-grid model for passenger evacuation in ships." *Journal of Marine Science and Application*, 10 (3): 340-346.

Fang, Z. M., W. G. Song, J. Zhang, and H. Wu. 2012. "A multi-grid model for evacuation coupling with the effects of fire products." *Fire Technology*, 48 (1): 91-104.

Guo, R. Y., H. J. Huang, and S. C. Wong. 2013 "A potential field approach to the modeling of route choice in pedestrian evacuation." *Journal of Statistical Mechanics: Theory and Experiment*, 2013 (2): P02010.

Hartmann, D. 2010. "Adaptive pedestrian dynamics based on geodesics." *New Journal of Physics*, 12 (4): 043032.

Helbing, D. 2001. "Traffic and related self-driven many-particle systems." *Reviews of Modern Physics*, 73 (4): 1067.

Helbing, D., A. Johansson, and H. Z. Al-Abideen. 2007. "Dynamics of crowd disasters: An empirical study." *Physical Review E*, 75 (4): 046109.

Helbing, D., and P. Molnár. 1995. "Social force model for pedestrian dynamics." *Physical Review E*, 51 (5): 4282.

Helbing, D., and P. Mukerji. 2012. "Crowd disasters as systemic failures: Analysis of the Love Parade disaster." *EPJ Data Science*, 1 (1): 7.

Helbing, D., P. Molnár, I. J. Farkas, and K. Bolay. 2001. "Self-organizing pedestrian movement." *Environment and Planning B: Planning and Design*, 28 (3): 361-383.

Hoogendoorn, S. P., and P. H. L. Bovy. 2004. "Pedestrian route-choice and activity scheduling theory and models." *Transportation Research Part B: Methodological* 38 (2): 169-190.

Huang, H. J., and W. H. K. Lam. 2002. "Modeling and solving the dynamic user equilibrium route and departure time choice problem in network with queues." *Transportation Research Part B: Methodological*, 36 (3): 253-273.

Huang, H. J., and R. Y. Guo. 2008. "Static floor field and exit choice for pedestrian evacuation in rooms with internal obstacles and multiple exits." *Physical Review E*, 78 (2): 021131.

Huang, L., S. C. Wong, M. Zhang, C. W. Shu, and W. H. K. Lam. 2009. "Revisiting Hughes' dynamic continuum model for pedestrian flow and the development of an efficient solution algorithm." *Transportation Research Part B: Methodological*, 43 (1): 127-141.

Hughes, R. L. 2002. "A continuum theory for the flow of pedestrians." *Transportation Research Part B: Methodological* 36 (6): 507-535.

Hussein, M., and T. Sayed. 2017. "A bi-directional agent-based pedestrian microscopic model." *Transportmetrica A: Transport Science* 13 (4): 326–355.

Ibrahim, A. M., I. Venkat, and P. De Wilde. 2018. "The impact of potential crowd behaviours on emergency evacuation: An evolutionary game theoretic approach." *Journal of Artificial Societies and Social Simulation*, 22 (1).

Jian, X. X., S. C. Wong, P. Zhang, K. Choi, H. Li, and X. Zhang. 2014. "Perceived cost potential field cellular automata model with an aggregated force field for pedestrian dynamics." *Transportation Research Part C: Emerging Technologies*, 42, 200-210.

Jiang, Y. Q., P. Zhang, S. C.Wong, and R. X. Liu. 2010. "A higher-order macroscopic model for

pedestrian flows." *Physica A: Statistical Mechanics and Its Applications*, 389 (21): 4623-4635.
Kielar, P. M., D. H. Biedermann, A. Kneidl, and A. Borrmann. 2018. "A unified pedestrian routing model for graph-based wayfinding built on cognitive principles." *Transportmetrica A: Transport Science* 14 (5-6): 406–432.
Kirchner, A., and A. Schadschneider. 2002. "Simulation of evacuation processes using a bionics-inspired cellular automaton model for pedestrian dynamics." *Physica A: Statistical Mechanics and Its Applications*, 312 (1-2): 260-276.
Kirchner, A., H. Klüpfel, K. Nishinari, A. Schadschneider, and M. Schreckenberg. 2004. "Discretization effects and the influence of walking speed in cellular automata models for pedestrian dynamics." *Journal of Statistical Mechanics: Theory and Experiment*, 2004 (10): P10011.
Kirchner, A., K. Nishinari, and A. Schadschneider. 2003. "Friction effects and clogging in a cellular automaton model for pedestrian dynamics." *Physical Review E*, 67 (5): 056122.
Kirik, E., T. Y. Yurgel'yan, and D. Krouglov. 2009. "The shortest time and/or the shortest path strategies in a CA FF pedestrian dynamics model." *Journal of Siberian Federal University. Mathematics and Physics*, 2 (3): 271-278.
Kretz, T. 2009. "Pedestrian traffic: On the quickest path." *Journal of Statistical Mechanics: Theory and Experiment*, 2009 (03): P03012.
Kretz, T. 2010. "The dynamic distance potential field in a situation with asymmetric bottleneck capacities." *International Conference on Cellular Automata*, Springer, Berlin, Heidelberg, 480-488.
Kretz, T., A. Grünebohm, and M. Schreckenberg. 2006. "Experimental study of pedestrian flow through a bottleneck." *Journal of Statistical Mechanics: Theory and Experiment*, 2006 (10): P10014.
Kuang, H., T. Chen, X. L. Li, and S. M. Lo. 2014. "A new lattice hydrodynamic model for bidirectional pedestrian flow considering the visual field effect." *Nonlinear Dynamics*, 78 (3): 1709-1716.
Kuang, H., X. Li, T. Song, and S. Dai. 2008. "Analysis of pedestrian dynamics in counter flow via an extended lattice gas model." *Physical Review E*, 78 (6): 066117.
Li, X., and L. Dong. 2012. "Modeling and simulation of pedestrian counter flow on a crosswalk." *Chinese Physics Letters*, 29 (9): 098902.
Lo, H. K., and A. Chen. 2000. "Traffic equilibrium problem with route-specific costs: Formulation and algorithms." *Transportation Research Part B: Methodological*, 34 (6): 493-513.
Müller, K. 1981. "Zur Gestaltung und Bemessung von Fluchtwegen für die Evakuierung von Personen aus Bauwerken auf der Grundlage von Modellversuchen." PhD diss, Verlag nicht ermittelbar.
Nishinari, K., A. Kirchner, A. Namazi, and A. Schadschneider. 2004. "Extended floor field CA model for evacuation dynamics." *IEICE Transactions on Information and Systems*, 87 (3): 726-732.
Nowak, S., and A. Schadschneide. 2012. "Quantitative analysis of pedestrian counterflow in a cellular automaton model." *Physical Review E* 85: 066128.
Porter, E., S. H. Hamdar, and W. Daamen. 2018. "Pedestrian dynamics at transit stations: an integrated pedestrian flow modeling approach." *Transportmetrica A: Transport Science* 14 (5-6): 468–483.
Sethian, J. A. 1999. "Fast marching methods." *SIAM Review*, 41 (2): 199-235.
Seyfried, A., O. Passon, B. Steffen, M. Boltes, T. Rupprecht, and W. Klingsch. 2009. "New insights into pedestrian flow through bottlenecks." *Transportation Science*, 43 (3): 395-406.
Song, W., X. Xu, B. H. Wang, and S. Ni. 2006. "Simulation of evacuation processes using a multi-grid model for pedestrian dynamics." *Physica A: Statistical Mechanics and Its Applications*, 363 (2): 492-500.
Szeto, W. Y., and S. C. Wong. 2012. "Dynamic traffic assignment: model classifications and recent advances in travel choice principles." *Central European Journal of Engineering*, 2 (1): 1-18.
Varas, A., M. D. Cornejo, D. Mainemer, B. Toledo, J. Rogan, V. Munoz, and J. A. Valdivia. 2007. "Cellular automaton model for evacuation process with obstacles." *Physica A: Statistical Mechanics and Its Applications*, 382 (2): 631-642.
Weng, W. G., L. L. Pan, S. F. Shen, and H. Y. Yuan. 2007. "Small-grid analysis of discrete model for evacuation from a hall." *Physica A: Statistical Mechanics and Its Applications*, 374 (2): 821-826.
Wong, S. C., W. L. Leung, S. H. Chan, W. H. K. Lam, N. H. Yung, C. Y. Liu, and P. Zhang. 2010.

"Bidirectional pedestrian stream model with oblique intersecting angle." *Journal of Transportation Engineering*, 136 (3): 234-242.

Xia, Y., S. C. Wong, and C. W. Shu. 2009. "Dynamic continuum pedestrian flow model with memory effect." *Physical Review E*, 79 (6): 066113.

Xie, D.F., Z. Y. Gao, X. M. Zhao, and D. Z. W. Wang. 2012. "Agitated behavior and elastic characteristics of pedestrians in an alternative floor field model for pedestrian dynamics." *Physica A: Statistical Mechanics and Its Applications*, 391 (7): 2390-2400.

Xie, S., and S. C. Wong. 2015. "A Bayesian inference approach to the development of a multidirectional pedestrian stream model." *Transportmetrica A: Transport Science* 11 (1): 61-73.

Xiong, T., P. Zhang, S. C. Wong, C. W. Shu, and M. Zhang. 2011. "A macroscopic approach to the lane formation phenomenon in pedestrian counter flow." *Chinese Physics Letters*, 28 (10): 108901.

Zhang, J., W. Song, and X. Xu. 2008. "Experiment and multi-grid modeling of evacuation from a classroom." *Physica A: Statistical Mechanics and Its Applications*, 387 (23): 5901-5909.

Zhang, P., X. X. Jian, S. C. Wong, and K. Choi. 2012. "Potential field cellular automata model for pedestrian flow." *Physical Review E*, 85 (2): 021119.

Zhao, H. 2005. "A fast sweeping method for eikonal equations." *Mathematics of Computation*, 74 (250): 603-627.

Zhou, Z., Y. Zhou, Z. Pu, and Y. Xu. 2019. "Simulation of pedestrian behavior during the flashing green signal using a modified social force model." *Transportmetrica A: Transport Science* 15 (2): 1019-1040.